

PAPER

[View Article Online](#)
[View Journal](#) | [View Issue](#)Cite this: *Dalton Trans.*, 2023, **52**,
8601

Why a simple vanadate is inefficient as a catalyst in the oxidation of alkanes with H₂O₂ – the long-standing puzzle is solved†‡

Maxim L. Kuznetsov * and Armando J. L. Pombeiro 

In contrast to V(v) complexes with various organic ligands, a simple vanadate without any additive is inactive in neutral medium toward the oxidation of alkanes with H₂O₂. In this work, we discovered that the insufficient activation of H₂O₂ upon coordination to the simple vanadate – the commonly accepted reason for the low catalytic activity of the vanadate – cannot explain this phenomenon. Two main findings are reported here on the basis of DFT calculations. First, the generally accepted Fenton-like mechanism of the generation of the active oxidizing species (HO•) in a vanadate/H₂O_{2(aq)}/MeCN system was revisited. A new mechanism based on the tremendous activation of the OOH ligand in the intermediate [V(OO)₂(OOH)(H₂O)] toward the homolytic O–O bond cleavage is not only feasible but significantly more favourable than the Fenton-like pathway. The surprisingly low activation barrier calculated for the HO• generation (15.4 kcal mol^{−1}) demonstrates the efficiency of this process. The presence of easily oxidizable non-innocent OO ligands in this intermediate explains such an activation. Second, it was found that the generated HO• radicals may be easily captured by the V atom soon after their formation followed by the elimination of the molecular oxygen. This side reaction of the H₂O₂ dismutation efficiently consumes the produced HO• radicals decreasing their concentration in the reaction mixture and preventing the following oxidation of alkanes.

Received 29th March 2023,
Accepted 18th May 2023

DOI: 10.1039/d3dt00967j

rsc.li/dalton

Introduction

Alkanes represent a cheap and abundant carbon raw material, and their functionalization into various valuable organic products is of tremendous importance.^{1–13} The main challenge associated with such transformations is the high chemical inertness of alkanes that requires the application of catalysts and strong oxidants. One of the most popular types of the catalysts used for the oxidation of alkanes is based on transition metal complexes or oxides. Vanadium is an element exhibiting several non-zero oxidation states, which permits its easy participation in various redox processes and enables broad applications of this element and its compounds in a number of catalytic reactions with the involvement of electron transfer (for reviews see ref. 13–33). Being the 6th most abundant transition metal on Earth, vanadium is quite cheap, and its usage as a catalyst is attractive from the economic point of view.

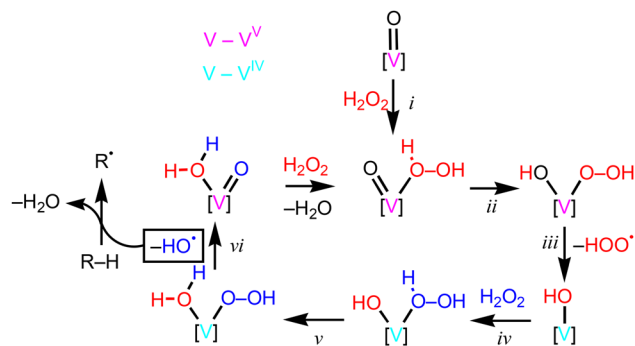
Several vanadium complexes with organic ligands (*e.g.* quinolin-8-olate, pyridine-2-carboxylate, triethanolamine, bipyridines, phenanthrolines, terephthalohydrazides, NO₂-donor Schiff bases, *etc.*) demonstrated a high catalytic activity in the oxidation of alkanes with hydrogen peroxide.^{34–38} Moreover, the simple vanadate VO₃[−] was found to be active in these processes but only in the presence of either an appropriate additive (*e.g.* pyrazine-2-carboxylic acid, PCAH)^{36,39} or a strong acid.⁴⁰ In the first case, the *in situ* formation of V-complexes with the additive occurs in solution, and these complexes serve as active catalytic forms. In the second case, the acidic medium provokes oligomerization of the vanadate, and the active catalytic form is divanadate.

The generally accepted Fenton-like mechanism includes (i) the formation of the H₂O₂ adduct with a catalyst molecule, (ii) proton transfer leading to a hydroperoxo intermediate, (iii) elimination of the HOO• radical with the reduction of the vanadium atom to V(IV), (iv) formation of the second H₂O₂ adduct, (v) second H-transfer and (vi) elimination of the HO• radical with the oxidation of the V(IV) atom³⁹ (Scheme 1). The formed HO• radical directly oxidizes an alkane molecule *via* a hydrogen atom abstraction. The key feature of this mechanism is the direct participation of the metal centre in the electron transfer processes. At the HOO• generation step, the V(v) atom

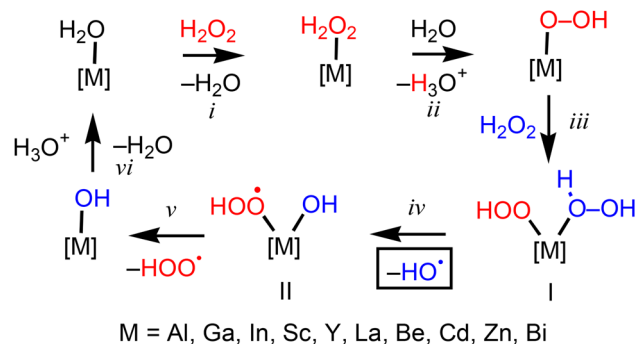
Centro de Química Estrutural, Institute of Molecular Sciences, Departamento de Engenharia Química, Instituto Superior Técnico, Universidade de Lisboa, Av. Rovisco Pais, 1049-001 Lisboa, Portugal. E-mail: max@mail.ist.utl.pt

† Dedicated to the memory of Prof. Georgiy B. Shul'pin.

‡ Electronic supplementary information (ESI) available. See DOI: <https://doi.org/10.1039/d3dt00967j>



Scheme 1 Generally accepted mechanism of HO[•] formation from H₂O₂ catalysed by V(v) complexes.



Scheme 2 Non-innocent ligand mechanism of HO[•] formation from H₂O₂ catalysed by salts of SSOS metals.

serves as an oxidant, while at the HO[•] formation step, the V(IV) centre is a reducing agent.

Meanwhile, the simple monomeric vanadate without any additive in the neutral medium – reaction conditions most attractive from the economic and environmental viewpoints – is not active toward the oxidation of alkanes with H₂O₂.^{39,41} The commonly accepted reason is the insufficient activation of H₂O₂ by the vanadate toward HO[•] production that leads to a high activation barrier for this process. It is expected that the introduction of an appropriate organic ligand or a second vanadate unit (in the case of divanadate) into the vanadate molecule increases the potential of the catalyst to activate H₂O₂ and decreases the activation energy. However, to the best of our knowledge, this hypothesis was never proved either experimentally or theoretically.

Recently, the authors paid attention to the fact that inorganic salts of some metals bearing only a single stable non-zero oxidation state (SSOS metals such as Al, Ga, Zn, *etc.*) are quite active as catalysts for the oxidation of alkanes with H₂O₂.^{42–44} The mechanism of a principally new type was proposed for these systems. This mechanism is based on the participation of a non-innocent (redox active) ligand in the catalyst molecule (or intermediate), whereas the metal oxidation state is not altered (the “non-innocent ligand mechanism”). It includes (i) the formation of a H₂O₂ adduct with the catalyst molecule, (ii) deprotonation of H₂O₂, (iii) addition of a second H₂O₂ molecule to give a key intermediate **I** bearing simultaneously the H₂O₂ and OOH[−] ligands and (iv) homolytic HO–OH bond cleavage in the H₂O₂ molecule affording HO[•] and complex **II** with the hydroperoxyl radical ligand (Scheme 2). The OOH[−] ligand in **I** is non-innocent and undergoes intramolecular oxidation upon HO–OH bond rupture. This oxidation stabilizes one of the products of the coordinated H₂O₂ decomposition and enables tremendous activation of H₂O₂ toward homolysis.

The non-innocent nature of the carbonate ligand and the hydrogen peroxide molecule in the Fenton like process between [Co(H₂O)₆]²⁺ and H₂O₂ as well as the non-innocent character of the Cp ligand in the radical generation from the complexes [Cp₂Ti(η¹-OO^tBu)L] (L = Cl[−], OTf[−], Br[−], OEt₂, Et₃P) were also previously reported.^{45–48}

The initial goal of this study was two-fold, *i.e.* (i) to confirm (or disprove) that the HO[•] generation from H₂O₂ catalysed by the simple vanadate has a high activation barrier and, for this reason, this catalyst is not active and (ii) to verify if the non-innocent ligand mechanism may effectively operate also for catalysts with a metal exhibiting various oxidation states (such as vanadium) or if it is feasible only for the SSOS metals.

The results obtained demonstrated that the non-innocent ligand mechanism is not only feasible but more favourable than the conventionally accepted pathway, and the latter should be revisited. Another unexpected finding indicated that the low activity of the simple vanadate in this reaction is associated not with a high activation barrier of the HO[•] generation but with an efficient side reaction of H₂O₂ decomposition into O₂ and H₂O catalysed by vanadate. The results of this study are described and discussed below.

Computational details

The full geometry optimization of all structures and transition states (TS) has been carried out at the density functional theory (DFT) level using the PBE0 functional⁴⁹ with the atom-pairwise dispersion correction and the Becke–Johnson damping scheme D3BJ⁵⁰ with the help of the Gaussian-09 program package.⁵¹ Recently, this functional demonstrated the excellent performance in the theoretical treatment of the activation of various main group bonds with (Ni,Pd)-based transition metal catalysts.⁵² The geometry optimization was performed by using the aug-cc-pVDZ basis set for all atoms with consideration of the solvent effects applying the polarizable continuum model in the “solvent model of density” (SMD) version⁵³ with acetonitrile as the solvent typically used in the experimental studies of the alkane oxidation with H₂O₂ catalysed by V species.^{34,36–40} Cartesian d and f basis functions (6d, 10f) were used in all calculations. No symmetry operations have been applied for any of the structures calculated. Singlet biradical structures were calculated using the broken symmetry approach^{54–56} applied with the Guess = Mix Gaussian keyword.



The Hessian matrix was calculated analytically for the optimized structures in order to prove the location of correct minima (no imaginary frequencies) or saddle points (only one imaginary frequency), and to estimate the thermodynamic parameters, the latter being calculated at a 298.15 K temperature and 1 atm pressure. The nature of all transition states was investigated by the analysis of vectors associated with the imaginary frequency and by the calculations of the intrinsic reaction coordinates (IRC) using the Gonzalez–Schlegel method.^{57–59}

All possible geometrical isomers were calculated for all V complexes, and the most stable isomers are discussed (if not stated otherwise).

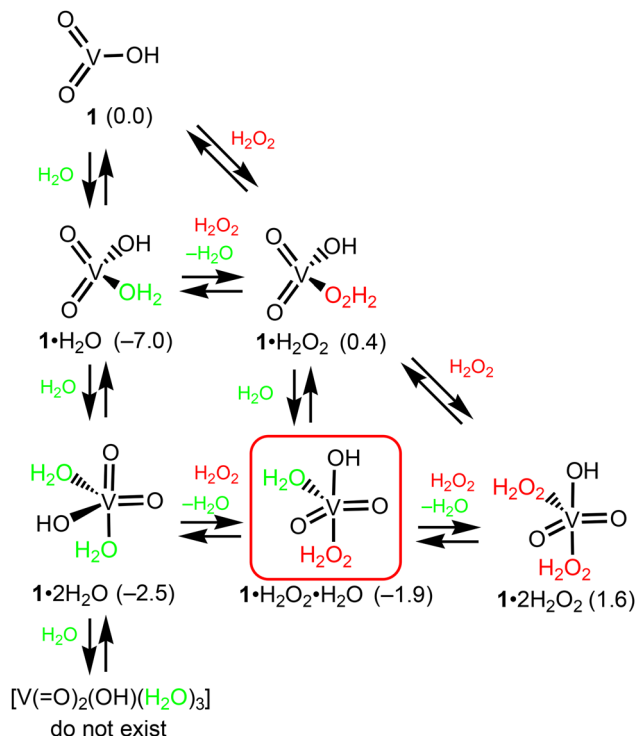
Results

In this section, first, equilibria in the vanadate/H₂O₂(aq)/MeCN catalytic system and the nature of the active catalytic species are discussed; second, the conventional mechanism of HO[•] formation from H₂O₂ catalysed by the simple vanadate is analysed; third, the feasibility of the non-innocent ligand mechanisms is discussed; and fourth, the reasons for the low activity of the simple vanadate in the generation of the HO[•] radicals are uncovered.

Equilibria in the vanadate/H₂O₂(aq)/MeCN system

Initial adducts. The reaction between the vanadate and hydrogen peroxide involves a series of H₂O₂ addition/substitution steps and proton transfers. In a solution bearing aqueous hydrogen peroxide, the coordination sphere of the vanadate HVO₃ may be saturated by water and/or H₂O₂ molecule(s). Equilibria between HVO₃ and the simple H₂O and/or H₂O₂ adducts are shown in Scheme 3. Among the aqua complexes, the most thermodynamically stable adduct is [V(=O)₂(OH)(H₂O)] (**1·H₂O**) with a tetrahedral arrangement of the ligands which contains one water molecule, while the octahedral complexes [V(=O)₂(OH)(H₂O)₃] (**1·3H₂O**) do not exist. In contrast, the most stable form of the H₂O₂ adduct is the trigonal bipyramid complex [V(=O)₂(OH)(H₂O₂)(H₂O)] (**1·H₂O₂·H₂O**) and this complex is the first reactive species toward the formation of the peroxo and diperoxo complexes of vanadium.

Formation of the monoperoxo complexes. Due to the acidic nature of the coordinated H₂O₂ in **1·H₂O₂·H₂O**, this molecule can lose a proton as a result of the intramolecular H-transfer either to one of the oxo-ligands to give [V(=O)(OH)₂(OOH)(H₂O)] (**2·H₂O**) or to the OH ligand affording [V(=O)₂(OOH)(H₂O)₂] (**3·2H₂O**) (Scheme 4). The latter pathway is slightly more kinetically favourable. The H-transfer occurs with the assistance of a water molecule which stabilizes the 6-membered transition states **TS1** and **TS2** (Fig. 1). The effect of water on the H-transfer in V-species has previously been discussed in detail.^{36,40} For both channels, the following water liberation results in more stable tetrahedral complexes **2** and **3·H₂O**. Among all the mentioned hydroperoxo complexes, **2** is the



Scheme 3 Equilibria between HVO₃ and water or hydrogen peroxide adducts (Gibbs free energies are indicated in parentheses in kcal mol^{−1} relative to that of HVO₃, and the most stable H₂O₂ adduct is boxed; here and further, only the most stable geometrical isomers are shown).

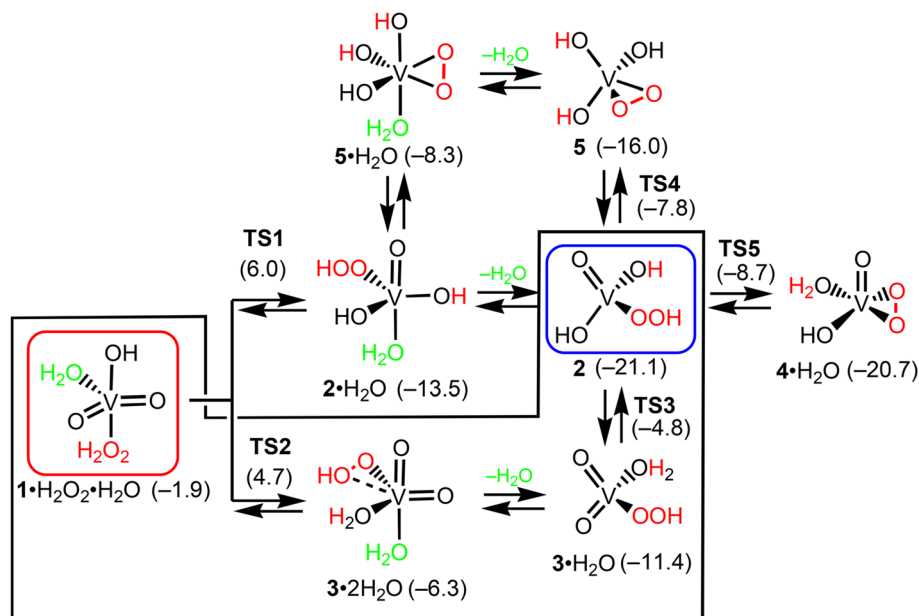
most stable one and it is formed through the **1·H₂O₂·H₂O** → **3·2H₂O** → **3·H₂O** → **2** pathway. The second H-transfer in **2** from the OOH ligand either to the hydroxo or to the oxo ligand leads to the formation of the monoperoxo complex [V(=O)(OH)(OO)(H₂O)] (**4·H₂O**) or [V(OH)₃(OO)] (**5**), respectively. The first process is both kinetically and thermodynamically more feasible.

Formation of the diperoxo complexes. This process starts with the associative substitution of H₂O for H₂O₂ in **4·H₂O** followed by the proton transfer which can occur to one of the =O, OH or OOH ligands in **4·H₂O₂** (Scheme 5). The calculations indicate that the most favourable route is the **4·H₂O** → **4·H₂O₂** → **7** → **6·H₂O** one. The second H-transfer affords the diperoxo species [V(OH)(OO)₂(H₂O)] (**9·H₂O**). Finally, one more substitution of H₂O for H₂O₂ in **9·H₂O** and the proton transfer yield the hydroperoxo diperoxo complex [V(OOH)(OO)₂(H₂O)] (**10·H₂O**). The last two species are the most thermodynamically stable ones in the vanadate/H₂O₂(aq)/MeCN system. The discussed equilibria are easily established, and the activation barriers for the formation of the most stable intermediates do not exceed 12.4 kcal mol^{−1}.

Conventional Fenton-like mechanism of HO[•] generation

The general scheme of the currently accepted Fenton-like mechanism of HO[•] radical formation from H₂O₂ catalysed by a V(v) species was discussed in Introduction and it is shown in





Scheme 4 Mechanisms of the formation of monoperoxo complexes (Gibbs free energies are indicated in parentheses in kcal mol⁻¹ relative to that of HVO₃; the initial and final species of this step and the most plausible pathway are indicated).

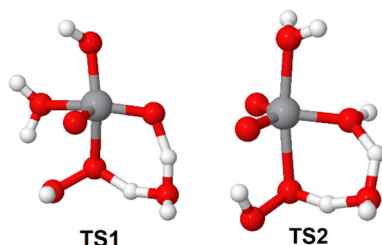
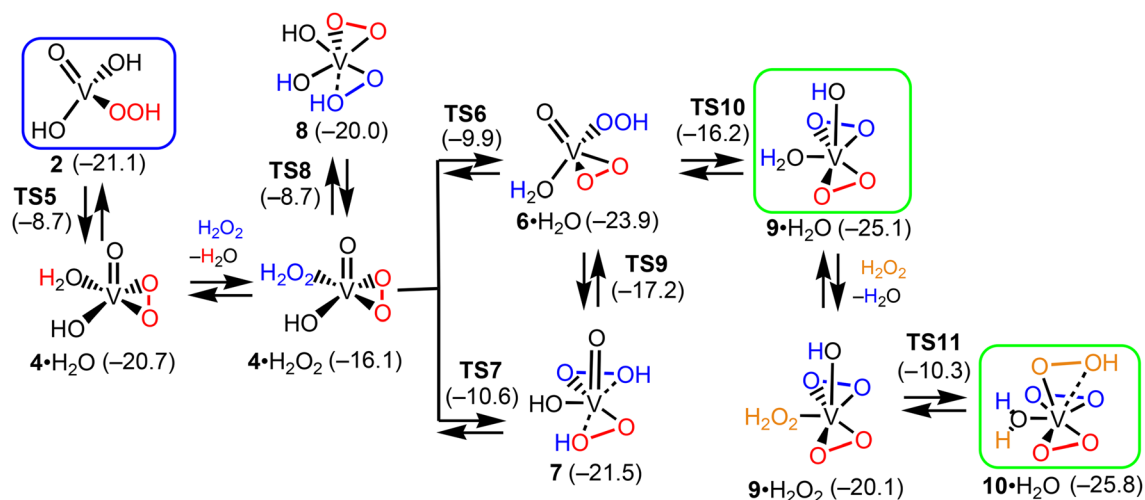


Fig. 1 Equilibrium structures of TS1 and TS2.

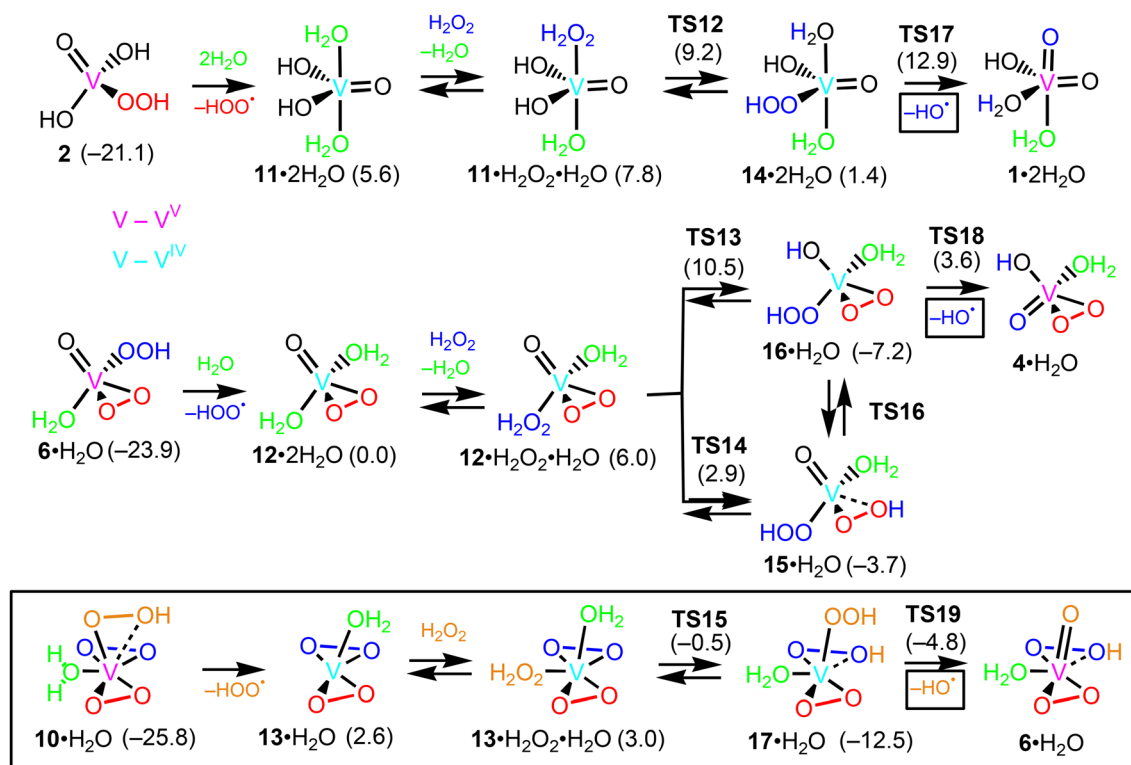
Scheme 1. The active catalytic forms in the vanadate/H₂O_{2(aq)}/MeCN system, which initiate this mechanism, are the V(v) hydroperoxo complexes **2**, **6**·H₂O and **10**·H₂O.

The HOO' formation step. Elimination of the HOO' radical from the hydroperoxo species upon V-OOH bond cleavage affords the reduced V(IV) complexes [V(=O)(OH)₂(H₂O)₂] (**11**·H₂O), [V(=O)(OO)(H₂O)₂] (**12**·H₂O) and [V(OO)₂(H₂O)] (**13**·H₂O) (Scheme 6). In the case of complexes **2** and **6**·H₂O, this process occurs *via* an associative mode including initial addition of two or one H₂O molecules, respectively, and the



Scheme 5 Mechanisms of the formation of diperoxo complexes (Gibbs free energies are indicated in parentheses in kcal mol⁻¹ relative to that of HVO₃; the initial species of this step and the most stable complexes in the vanadate/H₂O_{2(aq)}/MeCN system are boxed).





Scheme 6 Conventional mechanisms of HO^\bullet generation (Gibbs free energies are indicated in parentheses in kcal mol^{-1} relative to that of HVO_3 , and the most favourable pathway is boxed).

following HOO^\bullet elimination (Scheme S1 in the ESI†). In the case of complex $10\cdot\text{H}_2\text{O}$, the HOO^\bullet generation is realized dissociatively. The V–OOH bond cleavage is accompanied by the monotonous increase of the total energy of the system. The potential energy surface (PES) scan in $6\cdot\text{H}_2\text{O}$ indicates that until a V–OOH distance of *ca.* 2.41 Å is achieved, the singlet closed shell configuration is the most stable one (Fig. 2, left). At a longer distance, the singlet biradical configuration with unpaired electrons localized at the V atom and the leaving OOH group becomes more stable (Fig. 2, right).

The HO^\bullet formation step. At this step, the hydrogen peroxide adducts $[\text{V}(=\text{O})(\text{OH})_2(\text{H}_2\text{O}_2)(\text{H}_2\text{O})]$ ($11\cdot\text{H}_2\text{O}_2\cdot\text{H}_2\text{O}$), $[\text{V}(=\text{O})(\text{OO})(\text{H}_2\text{O}_2)(\text{H}_2\text{O})]$ ($12\cdot\text{H}_2\text{O}_2\cdot\text{H}_2\text{O}$) and $[\text{V}(\text{OO})_2(\text{H}_2\text{O}_2)(\text{H}_2\text{O})]$ ($13\cdot\text{H}_2\text{O}_2\cdot\text{H}_2\text{O}$) are formed upon water substitution for H_2O_2 or addition of H_2O_2 (Scheme 6). The subsequent proton transfer from the coordinated H_2O_2 molecule can occur to the oxo, hydroxo or peroxy ligand furnishing the hydroperoxo V(IV) complexes $[\text{V}(=\text{O})(\text{OH})(\text{OOH})(\text{H}_2\text{O})_2]$ ($14\cdot\text{H}_2\text{O}$), $[\text{V}(\text{OH})(\text{OOH})(\text{OO})(\text{H}_2\text{O})]$ ($16\cdot\text{H}_2\text{O}$) and $[\text{V}(\text{OOH})_2(\text{OO})(\text{H}_2\text{O})]$ ($17\cdot\text{H}_2\text{O}$). The formation of $16\cdot\text{H}_2\text{O}$ occurs in two steps *via* complex $15\cdot\text{H}_2\text{O}$. Finally, the O–O bond cleavage in the OOH ligand yields the HO^\bullet radical and restores the V(V) active catalytic forms.

The non-innocent ligand mechanisms of HO^\bullet generation

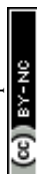
In this mechanism, the HO^\bullet radical is formed either from the OOH ligand in a V(V) complex or from the coordinated H_2O_2

molecule which are activated toward the O–O homolysis due to the presence of a non-innocent ligand in the complex.

Homolysis of the OOH ligand in the V(V) complexes. As discussed above, the establishing of the equilibria in the vanadate/ $\text{H}_2\text{O}_2(\text{aq})/\text{MeCN}$ system leads to the formation of three stable hydroperoxo V(V) complexes, *i.e.* $[\text{V}(=\text{O})(\text{OH})_2(\text{OOH})]$ (2), $[\text{V}(=\text{O})(\text{OOH})(\text{OO})(\text{H}_2\text{O})]$ ($6\cdot\text{H}_2\text{O}$) and $[\text{V}(\text{OOH})(\text{OO})_2(\text{H}_2\text{O})]$ ($10\cdot\text{H}_2\text{O}$).

Thermodynamic consideration. The dissociation of the OOH ligand in the first complex produces HO^\bullet and $[\text{V}(\text{O})_2(\text{OH})_2]$ (18) but it is endergonic by $35.9 \text{ kcal mol}^{-1}$ (Scheme 7). Such a high value is not surprising given that there is no non-innocent ligand in 2. This value is only by $2.0 \text{ kcal mol}^{-1}$ lower than that for the homolytic dissociation of free H_2O_2 ($37.9 \text{ kcal mol}^{-1}$).

A qualitatively different situation was found for the OOH homolyses in $6\cdot\text{H}_2\text{O}$ and $10\cdot\text{H}_2\text{O}$. In the former species, the ΔG° value of HO^\bullet formation is only $+5.8 \text{ kcal mol}^{-1}$, whereas in the latter complex, this process is *exergonic* by $-8.2 \text{ kcal mol}^{-1}$ indicating that the generation of HO^\bullet from $10\cdot\text{H}_2\text{O}$ is thermodynamically spontaneous. The reasons of such huge thermodynamic activation of OOH in these complexes become clear from the analysis of the products of this step, $[\text{V}(\text{O})_2(\text{OO})(\text{H}_2\text{O})]$ ($19\cdot\text{H}_2\text{O}$) and $[\text{V}(\text{O})(\text{OO})_2(\text{H}_2\text{O})]$ ($20\cdot\text{H}_2\text{O}$). The unpaired electron in these doublet species is localized at the OO ligand rather than at the V atom (Fig. 3). Thus, the HO^\bullet elimination does not result in a change of the V oxidation state which remains at +5. The



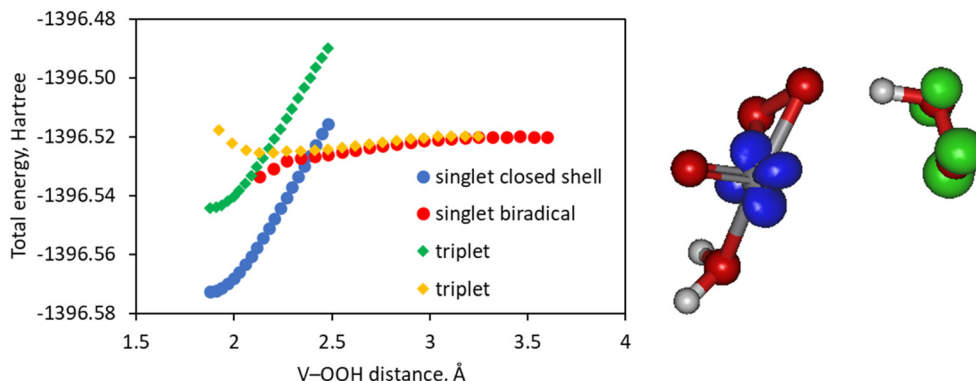
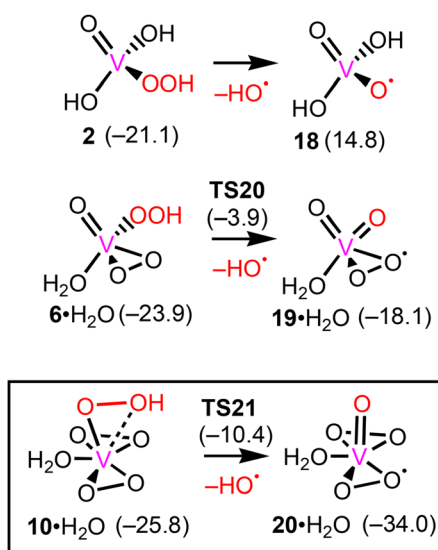


Fig. 2 PES scans for the elongation of the V–OOH bond in the complex **6·H₂O** (left, scans of two electronic triplet configurations are indicated) and a plot of spin density for the singlet biradical structure at a V–OOH distance of 3.6 Å (right).



Scheme 7 Formation of the HO[•] radical from the hydroperoxo V(v) complexes through the non-innocent ligand mechanism (Gibbs free energies are indicated in parentheses in kcal mol^{−1} relative to that of HVO₃, and the most favourable pathway is boxed).

homolytic VO–OH bond cleavage produces a free HO[•] radical and an oxyl anion-radical O^{•−} which is coordinated to V in **19·H₂O** or **20·H₂O**. During the O–O bond rupture, the coordinated O^{•−} anion-radical is reduced intramolecularly, oxidizing the OO ligand and not the V centre as in the V(IV) complexes **11·2H₂O**,

12·2H₂O and **13·H₂O** of the conventional mechanism. As a result, O^{•−} is transformed into the oxo ligand (=O)^{2−}, while the peroxo (OO)^{2−} ligand is oxidized into the peroxy species (OO)^{•−}. Therefore, the (OO)^{2−} ligand exhibits non-innocent behaviour which permits further oxidation of the V(v) complexes **6·H₂O** and **10·H₂O** despite them bearing the metal centre in its highest oxidation state. The ability of the (OO)^{2−} ligand to be easily oxidized is a driving force for the tremendous thermodynamic activation of OOH in the hydroperoxo V(v) complexes **6·H₂O** and **10·H₂O**.

Kinetic consideration. The low ΔG^o values of HO[•] formation from **6·H₂O** and **10·H₂O** allow the assumption that these processes are controlled by kinetic factors rather than by thermodynamic ones. The analysis of the kinetic features is not trivial in this case since the initial complexes are singlet close shell structures while both reaction products are doublets. Therefore, the PES scans for the VO–OH bond cleavage in **6·H₂O** and **10·H₂O** at different spin states were firstly analysed. At the singlet close shell PES, an increase of the VO–OH distance corresponding to the heterolytic VO–OH bond cleavage is accompanied by the monotonic enhancement of the system's energy (Fig. 4). This process is unfavourable, and the elongation of the VO–OH bond until 2 Å requires 30–33 kcal mol^{−1}.

The adiabatic excitation of **6·H₂O** with the unrelaxed VO–OH bond distance to the singlet biradical state ^{1,1}**6·H₂O** requires only 12.2 kcal mol^{−1}. One of the unpaired electrons in ^{1,1}**6·H₂O** is localized at the V atom while another one is mostly distributed among the peroxo ligand (Fig. 4A). The OOH

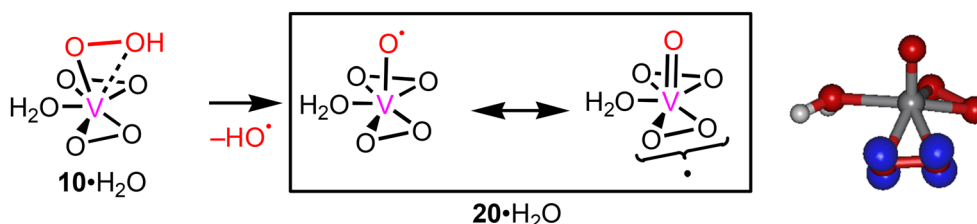


Fig. 3 O–OH bond cleavage in **10·H₂O**, intramolecular electron transfer and spin density distribution in **20·H₂O**.



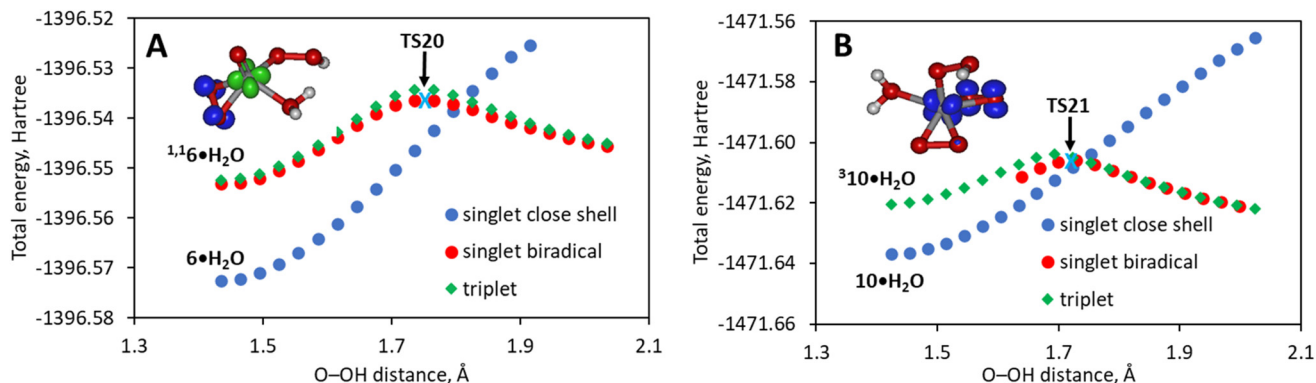


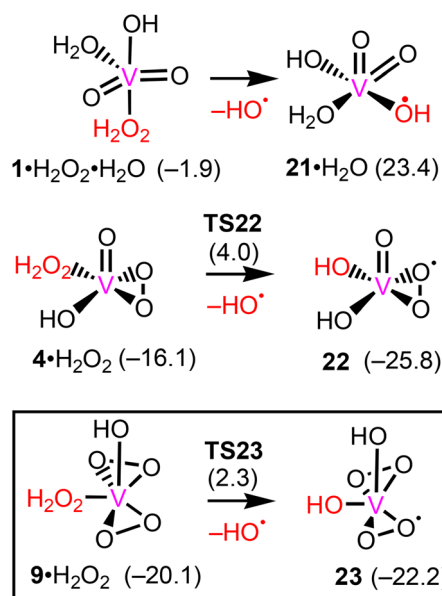
Fig. 4 PES scans for the elongation of the VO–OH bond in complexes $6\cdot\text{H}_2\text{O}$ (A) and $10\cdot\text{H}_2\text{O}$ (B) (positions of the equilibrium structures of TS20 and TS21 are shown by cross and plots of spin density for $^{1,1}6\cdot\text{H}_2\text{O}$ and $^{3,10}\cdot\text{H}_2\text{O}$ are provided).

ligand being bidentate in the ground state of $6\cdot\text{H}_2\text{O}$ becomes monodentate in $^{1,1}6\cdot\text{H}_2\text{O}$. The V–O(OO) bonds elongate upon excitation from 1.82–1.83 Å to 1.96–1.99 Å which corresponds to the formation of the peroxy ligand (OO) $^{\cdot-}$. Thus, this excitation results in the formation of a V(IV) species due to an intramolecular redox process between the metal centre and the OO ligand. Upon increase of the VO–OH distance, the total energy on the singlet biradical PES reaches the maximum at 1.74 Å and then decreases.

The PES character of the complex $10\cdot\text{H}_2\text{O}$ is similar (Fig. 4B). In this case, the singlet biradical structures could be calculated only for VO–OH distances longer than 1.63 Å. The initial excitation energy to the triplet state $^{3,10}\cdot\text{H}_2\text{O}$ is 10.4 kcal mol $^{-1}$. The excitation affects only one peroxy ligand.

With the help of PES scan results, the singlet biradical transition states TS20 and TS21 which correspond to the homolytic VO–OH bond cleavage in $6\cdot\text{H}_2\text{O}$ and $10\cdot\text{H}_2\text{O}$ were located (Fig. 5). The spin density in these TSs is mostly localized at the V atom ($\rho_{s,\alpha} = 0.81$ and $0.72e$), one OO ligand ($\rho_{s,\beta} = 1.05e$) and the oxygen atom of the leaving HO $^{\cdot}$ radical ($\rho_{s,\alpha} = 0.54$ and $0.53e$). Thus, the VO–OH bond rupture in the excited complexes $^{1,1}6\cdot\text{H}_2\text{O}$ and $^{1,1}10\cdot\text{H}_2\text{O}$ leads to the intramolecular reduction of the oxygen atom coordinated to the V atom to form the oxo ligand O $^{2-}$.

Homolysis of the coordinated H₂O₂. Coordination of H₂O₂ to the V(v) centre can activate this molecule toward homolysis and formation of the HO $^{\cdot}$ radical (Scheme 8). Three H₂O₂



Scheme 8 Formation of the HO $^{\cdot}$ radical from the hydrogen peroxide V(v) complexes through the non-innocent ligand mechanism (Gibbs free energies are indicated in parentheses in kcal mol $^{-1}$ relative to that of HVO₃, and the most favourable pathway is boxed).

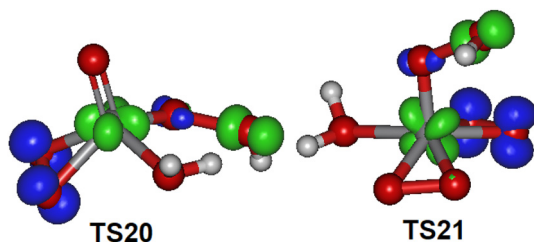


Fig. 5 Equilibrium structures and plots of spin densities for TS20 and TS21.

adducts can be formed in the vanadate/H₂O_{2(aq)}/MeCN system, *i.e.* [V(=O)₂(OH)(H₂O₂)(H₂O)] ($1\cdot\text{H}_2\text{O}_2\cdot\text{H}_2\text{O}$), [V(=O)(OH)(OO)(H₂O₂)] ($4\cdot\text{H}_2\text{O}_2$) and [V(OH)(OO)₂(H₂O₂)] ($9\cdot\text{H}_2\text{O}_2$). The decomposition of $1\cdot\text{H}_2\text{O}_2\cdot\text{H}_2\text{O}$ into HO $^{\cdot}$ and [V(=O)₂(OH)₂(H₂O)] ($21\cdot\text{H}_2\text{O}$) is not favourable due to the absence of any non-innocent ligands in this complex ($\Delta G^\circ = 25.3$ kcal mol $^{-1}$). In contrast, the homolysis of H₂O₂ in the other two adducts is exergonic by -9.7 and -2.1 kcal mol $^{-1}$ because of the presence of the redox active peroxy ligand. As in the case of the V(v) hydroperoxo species, the homolytic HO–OH bond cleavage in $4\cdot\text{H}_2\text{O}_2$ and $9\cdot\text{H}_2\text{O}_2$ results in the intramolecular oxidation of the redox active OO ligand to the OO $^{\cdot-}$ anion-radical and reduction of the formed coordinated OH group, while the oxidation state of vanadium remains intact.

The PES scan analysis allowed the localization of the singlet biradical transition states **TS22** and **TS23** corresponding to the homolytic HO–OH bond cleavage in **4-H₂O₂** and **9-H₂O₂** (Fig. S1 in ESI†). The spin density in **TS22** and **TS23** is mostly localized at the V atom, one peroxo ligand and the leaving HO• radical.

Activation energies and comparison of reaction mechanisms

The inspection of the calculated mechanisms indicates the following. First, in the solution of vanadate with aqueous hydrogen peroxide, several diperoxo, monoperoxo and hydroperoxo complexes are easily formed. The diperoxo complexes **9-H₂O** and **10-H₂O** are the most thermodynamically stable in such a solution, and they are in equilibrium with other slightly less stable monoperoxo and hydroperoxo complexes **6-H₂O**, **7**, **4-H₂O** and **2** (Scheme 5). The diperoxo and monoperoxo V(v) species were detected experimentally in the aqueous solution in the presence of H₂O₂ using the NMR technique.^{60–63}

Second, the most favourable pathway of the conventional mechanism is based on the hydroperoxo diperoxo complex **10-H₂O** and includes the sequence of steps **10-H₂O** → **13-H₂O** (+HOO•) → **13-H₂O₂·H₂O** → **17-H₂O** → **6-H₂O** (+HO•) (Scheme 6). The overall Gibbs free energy of activation for HO• formation in this pathway is 28.8 kcal mol^{−1} relative to **10-H₂O**. The rate determining step is the formation of the V(IV) hydrogen peroxide adduct **13-H₂O₂·H₂O**.

Third, the non-innocent ligand mechanism based on the simple homolysis of the OOH ligand in [V(OOH)(OO)₂(H₂O)] **10-H₂O** (Scheme 7) is significantly more favourable than the conventional mechanism. This pathway has an activation barrier of 15.4 kcal mol^{−1} relative to **10-H₂O**, and the rate limiting step is the VO–OH bond cleavage in **10-H₂O**.

Fourth, the non-innocent ligand mechanism based on the homolysis of H₂O₂ coordinated in [V(OH)(OO)₂(H₂O)] **9-H₂O** has an activation energy of 28.1 kcal mol^{−1} relative to **10-H₂O** which is comparable to that of the conventional mechanism (Scheme 8).

Fifth, the presence of two peroxo ligands in the catalytic complexes is crucial for the highest activation of the H₂O₂ and OOH ligands toward homolysis. All pathways based on the monoperoxo species **2** and **6-H₂O** require a higher activation barrier than the pathways of the same mechanism based on the diperoxo complex **10-H₂O**.

Thus, one of the most important results of this work is that *the mechanism involving the non-innocent peroxo ligand is not only feasible but also more favourable than the conventional Fenton-like mechanism.*

Why a simple vanadate is not efficient as a catalyst for the oxidation of alkanes with H₂O₂?

The calculated overall activation barrier for the most plausible mechanism of HO• generation is 15.4 and 17.4 kcal mol^{−1} in terms of the Gibbs free energy and enthalpy of activation, respectively. Such low values make the generation of the HO• radicals in the vanadate/H₂O_{2(aq)}/MeCN system quite efficient. The latter value correlates well with the experimental activation energy of HO• generation in the *n*-Bu₄NVO₃/PCAH/H₂O_{2(aq)}/

MeCN system which is active for the oxidation of alkanes (17 ± 2 kcal mol^{−1} (ref. 39)). Thus, the low activity of the simple vanadate (without any additive) as a catalyst in the oxidation of alkanes with H₂O₂ cannot be justified by the high activation energy for this process.

During the search for PES for the VO–OH bond cleavage in **10-H₂O** it was found that the liberating HO• radical can easily be trapped by the V atom soon after the formation of **TS21**. Indeed, the PES scan for the shortening of the V...OH_{leaving} distance starting from a point on the energy curve after **TS21** revealed a barrier of HO• capture of only 2.0 kcal mol^{−1} (Fig. 6, see the ESI† for details). As a result, the singlet biradical complex [V(=O)(OH)(OO)₂] (**^{1,1}24**) is formed that is accompanied by an extrusion of the water molecule initially coordinated in **10-H₂O**. The spin density in **^{1,1}24** is localized at two peroxo OO ligands (1.07e for each ligand, Fig. 7) which

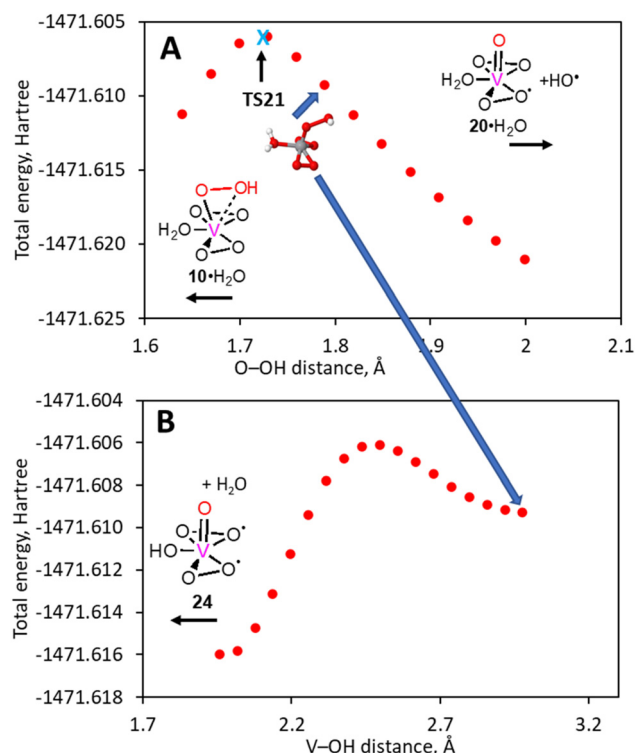


Fig. 6 Singlet biradical PES scans for the O–OH bond cleavage in **10-H₂O** (A) and for the shortening of the V...OH_{leaving} distance from one of the points on the reaction path after **TS21** (B).

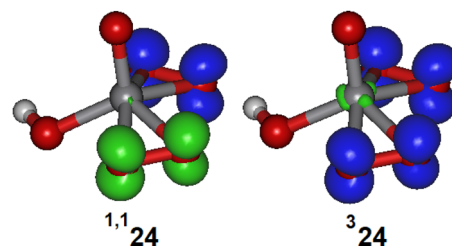
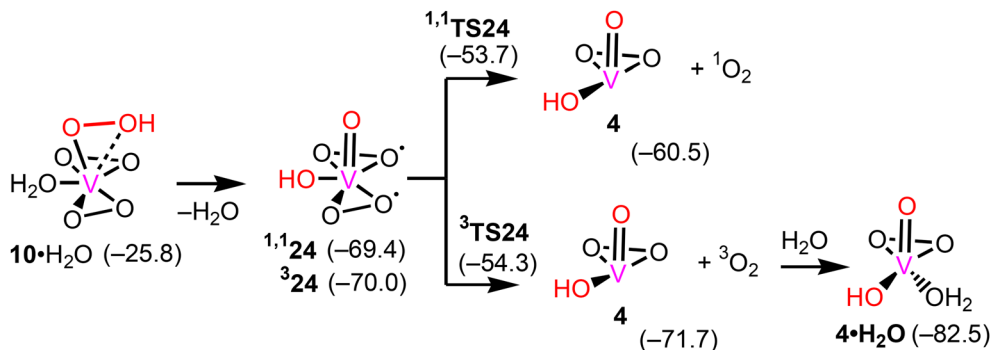


Fig. 7 Plots of spin density in **^{1,1}24** and **³24**.

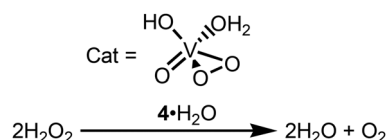




Scheme 9 HO[•] radical trap upon O–OH bond cleavage in 10•H₂O and the following liberation of O₂.

corresponds to the structure with two anion-radical peroxy ligands (OO)^{•−}. The spin conversion from the singlet biradical to the triplet state ³24 then occurs, the latter state being more stable by 0.6 kcal mol^{−1}. Both states have similar spin distribution with some involvement of the V atom in the case of the triplet structure.

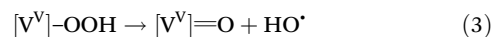
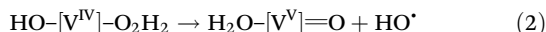
The formation of complex 24 from 10•H₂O is highly exergonic by (−43.6)–(−44.2) kcal mol^{−1} (Scheme 9). Both singlet biradical and triplet complexes 24 can easily lose the molecular oxygen affording the monoperoxo species [V(=O)(OH)(OO)] (4) which is stabilized by water addition to give 4•H₂O. The singlet biradical channel leads to the formation of the singlet oxygen which was detected experimentally in the reactions of the V(v) species with H₂O₂.⁶⁴ Upon these processes, one of the (OO)^{•−} ligands experiences further oxidation to O₂, whereas another (OO)^{•−} ligand is reduced to the peroxo ligand (OO)^{2−} (Fig. 8). The O₂ liberation has quite a low activation barrier of 15.7 kcal mol^{−1} and it is exergonic by −12.5 kcal mol^{−1}. Thus, the HO[•] radical trapping by the V centre is very efficient. Overall, this reaction channel corresponds to the catalytic dismutation of H₂O₂ into O₂ and H₂O (Scheme 10). The consumption of HO[•] in this side reaction significantly decreases the concentration of these radicals in the reaction mixture and makes their interaction with an alkane molecule inefficient.



Scheme 10 Dismutation of H₂O₂ catalysed by the complex 4•H₂O.

in the simple vanadate has been postulated as the reason for such low activity. However, to the best of our knowledge, no systematic studies aimed at supporting this assumption have been undertaken. In this article, the results of the detailed mechanistic study of HO[•] formation in the vanadate/H₂O₂(aq)/MeCN system are reported.

This work resulted in two unexpected discoveries which finally shed light on this issue. First, the commonly accepted mechanism of the vanadium(v) catalysed oxidation of alkanes with H₂O₂ represented in the most general form by eqn (1) and (2) was revisited. Another mechanism of HO[•] generation (eqn (3)) based on the participation of a non-innocent ligand – which was not previously considered for the V activation of H₂O₂ toward homolysis – was found to be not only feasible but also more favourable than the conventional mechanism.



This new mechanism starts with the formation of the hydroperoxo diperoxo complex [V(OOH)(OO)₂(H₂O)] 10•H₂O upon several H₂O-for-H₂O₂ substitution and H⁺-transfer steps – 10•H₂O being the most stable catalytic form in the vanadate/H₂O₂(aq)/MeCN system – and includes simple monomolecular homolytic VO–OH bond cleavage in 10•H₂O affording [V(=O)(OO)₂(H₂O)] 20•H₂O and HO[•] (Scheme 11). Despite the V atom being in its highest oxidation state in 10•H₂O, the further oxidation of the catalyst may occur upon VO–OH bond cleavage due to the presence of the non-innocent peroxo ligand which is oxidized instead of the metal centre. The reaction product 20•H₂O, thus, represents the V(v) species bearing one peroxy

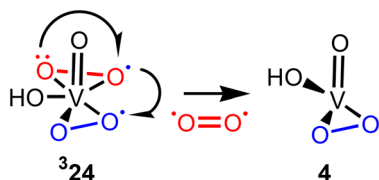
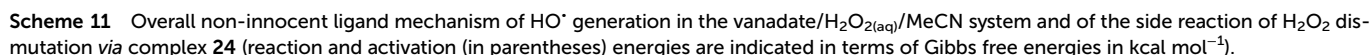


Fig. 8 Liberation of O₂ in complex ³24.



The role of the hydroperoxo V complexes as active catalytic species was revealed in the oxidation of halide anions with

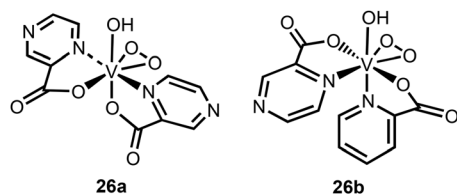
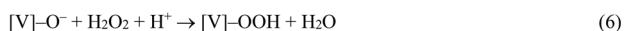
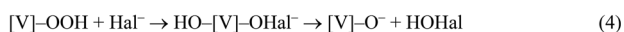


Chart 1

H₂O₂ catalysed by vanadium haloperoxidase enzymes or mimicking model complexes.^{66–69} In this reaction, the OOH ligand undergoes two-electron reduction by the Hal[–] anion while the latter is oxidized to the hypohalite anion OHal[–] which may be coordinated to the V atom (eqn (4)). The formed hypohalite oxidizes hydrogen peroxide to the molecular oxygen and water (eqn (5)), and the overall process corresponds to the dismutation of H₂O₂ (eqn. (4)–(7)).⁶⁷ In the case of the simple vanadate with an unsaturated coordination sphere, the generated HO[•] radicals serve as such oxidizing species.



Data availability

Additional data may be found in the ESI† or could be requested from the authors.

Author contributions

MLK – conceptualization of the work, computational studies, writing and preparation of the manuscript. AJLP – conceptualization of the work, discussion of results, proof reading, and funding.

Conflicts of interest

The authors declare no conflict of interest.

Acknowledgements

This work was partially supported by the Fundação para a Ciência e a Tecnologia (FCT), Portugal, projects UIDB/00100/2020 and UIDP/00100/2020 of Centro de Química Estrutural and LA/P/0056/2020 of Institute of Molecular Sciences.

References

- 1 A. E. Shilov and G. B. Shul'pin, *Chem. Rev.*, 1997, **97**, 2879.
- 2 G. B. Shul'pin, *Mini-Rev. Org. Chem.*, 2009, **6**, 95.
- 3 R. H. Crabtree, *Chem. Rev.*, 1995, **95**, 987.
- 4 C. Jia, T. Kitamura and Y. Fujiwara, *Acc. Chem. Res.*, 2001, **34**, 633.
- 5 B. S. Lane and K. Burgess, *Chem. Rev.*, 2003, **103**, 2457.
- 6 G. Grigoropoulou, J. H. Clark and J. A. Elings, *Green Chem.*, 2003, **5**, 1.
- 7 *Alkane Functionalization*, ed. A. J. L. Pombeiro and M. F. C. Guedes da Silva, J. Wiley & Sons, Hoboken, NJ, USA, 2019.
- 8 J. A. Labinger, *J. Mol. Catal. A: Chem.*, 2004, **220**, 27.
- 9 B. L. Conley, W. J. Tenn III, K. J. H. Young, S. K. Ganesh, S. K. Meier, V. R. Ziatdinov, O. Mironov, J. Oxgaard, J. Gonzales, W. A. Goddard III and R. A. Periana, *J. Mol. Catal. A: Chem.*, 2006, **251**, 8.
- 10 J. Muzart, *J. Mol. Catal. A: Chem.*, 2007, **276**, 62.
- 11 M. M. Díaz-Requejo and P. J. Pérez, *Chem. Rev.*, 2008, **108**, 3379.
- 12 R. H. Crabtree, *Chem. Rev.*, 2010, **110**, 575.
- 13 J. A. L. da Silva, J. J. R. Fraústo da Silva and A. J. L. Pombeiro, *Coord. Chem. Rev.*, 2011, **255**, 2232.
- 14 *Vanadium catalysis*, ed. M. Sutradhar, J. A. L. da Silva and A. J. L. Pombeiro, Royal Society of Chemistry, Cambridge, UK, 2021.
- 15 R. R. Langeslay, D. M. Kaphan, C. L. Marshall, P. C. Stair, A. P. Sattelberger and M. Delferro, *Chem. Rev.*, 2019, **119**, 2128.
- 16 K. Nomura and S. Zhang, *Chem. Rev.*, 2011, **111**, 2342.
- 17 P. Schwendt, J. Tatiersky, L. Krivosudský and M. Šimuneková, *Coord. Chem. Rev.*, 2016, **318**, 135.
- 18 V. Conte, A. Coletti, B. Floris, G. Licini and C. Zonta, *Coord. Chem. Rev.*, 2011, **255**, 2165.
- 19 A. M. F. Phillips, H. Suo, M. F. C. Guedes da Silva, A. J. L. Pombeiro and W.-H. Sun, *Coord. Chem. Rev.*, 2020, **416**, 213332.
- 20 M. Kirihaara, *Coord. Chem. Rev.*, 2011, **255**, 2281.
- 21 G. Licini, V. Conte, A. Coletti, M. Mba and C. Zonta, *Coord. Chem. Rev.*, 2011, **255**, 2345.
- 22 H. Hagen, J. Boersma and G. van Koten, *Chem. Soc. Rev.*, 2002, **31**, 357.
- 23 J.-Q. Wu and Y.-S. Li, *Coord. Chem. Rev.*, 2011, **255**, 2303.
- 24 H. Pellissier, *Coord. Chem. Rev.*, 2015, **284**, 93.
- 25 B. M. Weckhuysen and D. E. Keller, *Catal. Today*, 2003, **78**, 25.
- 26 N. F. Dummer, J. K. Bartley and G. J. Hutchings, *Adv. Catal.*, 2011, **54**, 189.
- 27 M. R. Maurya, A. Kumar and J. C. Pessoa, *Coord. Chem. Rev.*, 2011, **255**, 2315.
- 28 A. Chieragato, J. M. L. Nieto and F. Cavani, *Coord. Chem. Rev.*, 2015, **301–302**, 3.
- 29 J. C. Védrine, G. J. Hutchings and C. J. Kiely, *Catal. Today*, 2013, **217**, 57.
- 30 M. O. Guerrero-Pérez, *Catal. Today*, 2017, **285**, 226.



- 31 W. Chu, J. Luo, S. Paul, Y. Liu, A. Khodakov and E. Bordes, *Catal. Today*, 2017, **298**, 145.
- 32 N. Mizuno and K. Kamata, *Coord. Chem. Rev.*, 2011, **255**, 2358.
- 33 J. J. H. B. Sattler, J. Ruiz-Martinez, E. Santillan-Jimenez and B. M. Weckhuysen, *Chem. Rev.*, 2014, **114**, 10613.
- 34 I. Gryca, K. Czerwińska, B. Machura, A. Chrobok, L. S. Shul'pina, M. L. Kuznetsov, D. S. Nesterov, Y. N. Kozlov, A. J. L. Pombeiro, I. A. Varyan and G. B. Shul'pin, *Inorg. Chem.*, 2018, **57**, 1824.
- 35 H. Mimoun, L. Saussine, E. Daire, M. Postel, J. Fischer and R. Weiss, *J. Am. Chem. Soc.*, 1983, **105**, 3101.
- 36 M. V. Kirillova, M. L. Kuznetsov, V. B. Romakh, L. S. Shul'pina, J. J. R. Fraústo da Silva, A. J. L. Pombeiro and G. B. Shul'pin, *J. Catal.*, 2009, **267**, 140.
- 37 I. S. Fomenko, A. L. Gushchin, P. A. Abramov, M. N. Sokolov, L. S. Shul'pina, N. S. Ikonnikov, M. L. Kuznetsov, A. J. L. Pombeiro, Y. N. Kozlov and G. B. Shul'pin, *Catalysts*, 2019, **9**, 217.
- 38 M. Sutradhar, N. V. Shvydkiy, M. F. C. Guedes da Silva, M. V. Kirillova, Y. N. Kozlov, A. J. L. Pombeiro and G. B. Shul'pin, *Dalton Trans.*, 2013, **42**, 11791.
- 39 G. B. Shul'pin, Y. N. Kozlov, G. V. Nizova, G. Süss-Fink, S. Stanislas, A. Kitaygorodskiy and V. S. Kulikova, *J. Chem. Soc., Perkin Trans. 2*, 2001, 1351.
- 40 M. V. Kirillova, M. L. Kuznetsov, Y. N. Kozlov, L. S. Shul'pina, A. Kitaygorodskiy, A. J. L. Pombeiro and G. B. Shul'pin, *ACS Catal.*, 2011, **1**, 1511.
- 41 G. B. Shul'pin and G. Süss-Fink, *J. Chem. Soc., Perkin Trans. 2*, 1995, 1459.
- 42 M. L. Kuznetsov, Y. N. Kozlov, D. Mandelli, A. J. L. Pombeiro and G. B. Shul'pin, *Inorg. Chem.*, 2011, **50**, 3996.
- 43 A. S. Novikov, M. L. Kuznetsov, A. J. L. Pombeiro, N. A. Bokach and G. B. Shul'pin, *ACS Catal.*, 2013, **3**, 1195.
- 44 M. L. Kuznetsov, F. A. Teixeira, N. A. Bokach, A. J. L. Pombeiro and G. B. Shul'pin, *J. Catal.*, 2014, **313**, 135.
- 45 A. Burg, D. Shamir, I. Shusterman, H. Kornweitz and D. Meyerstein, *Chem. Commun.*, 2014, **50**, 13096.
- 46 A. Burg, I. Shusterman, H. Kornweitz and D. Meyerstein, *Dalton Trans.*, 2014, **43**, 9111.
- 47 A. G. DiPasquale, D. A. Hrovat and J. M. Mayer, *Organometallics*, 2006, **25**, 915.
- 48 A. G. DiPasquale, W. Kaminsky and J. M. Mayer, *J. Am. Chem. Soc.*, 2002, **124**, 14534.
- 49 C. Adamo and V. Barone, *J. Chem. Phys.*, 1999, **110**, 6158.
- 50 S. Grimme, S. Ehrlich and L. Goerigk, *J. Comput. Chem.*, 2011, **32**, 1456.
- 51 M. J. Frisch, G. W. Trucks, H. B. Schlegel, G. E. Scuseria, M. A. Robb, J. R. Cheeseman, G. Scalmani, V. Barone, B. Mennucci, G. A. Petersson, H. Nakatsuji, M. Caricato, X. Li, H. P. Hratchian, A. F. Izmaylov, J. Bloino, G. Zheng, J. L. Sonnenberg, M. Hada, M. Ehara, K. Toyota, R. Fukuda, J. Hasegawa, M. Ishida, T. Nakajima, Y. Honda, O. Kitao, H. Nakai, T. Vreven, J. A. Montgomery Jr., J. E. Peralta, F. Ogliaro, M. Bearpark, J. J. Heyd, E. Brothers, K. N. Kudin, V. N. Staroverov, R. Keith, J. Kobayashi, K. Normand, A. Raghavachari, J. C. Rendell, S. S. Burant, T. Iyengar, J. Tomasi, M. Cossi, N. Rega, J. M. Millam, M. Klene, J. E. Knox, J. B. Cross, V. Bakken, C. Adamo, J. Jaramillo, R. Gomperts, R. E. Stratmann, O. Yazyev, A. J. Austin, R. Cammi, C. Pomelli, J. W. Ochterski, R. L. Martin, K. Morokuma, V. G. Zakrzewski, G. A. Voth, P. Salvador, J. J. Dannenberg, S. Dapprich, A. D. Daniels, O. Farkas, J. B. Foresman, J. V. Ortiz, J. Cioslowski and D. J. Fox, *Gaussian 09, Rev. D.01*, Gaussian Inc., 2013.
- 52 M. Steinmetz and S. Grimme, *ChemistryOpen*, 2013, **2**, 115.
- 53 A. V. Marenich, C. J. Cramer and D. G. Truhlar, *J. Phys. Chem. B*, 2009, **113**, 6378.
- 54 L. Noodleman and D. A. Case, *Adv. Inorg. Chem.*, 1992, **38**, 423.
- 55 E. Ruiz, J. Cano, S. Alvarez and P. Alemany, *J. Comput. Chem.*, 1999, **20**, 1391.
- 56 E. Ruiz, A. Rodriguez-Forte, J. Cano, S. Alvarez and P. Alemany, *J. Comput. Chem.*, 2003, **24**, 982.
- 57 C. Gonzalez and H. B. Schlegel, *J. Chem. Phys.*, 1991, **95**, 5853.
- 58 C. Gonzalez and H. B. Schlegel, *J. Chem. Phys.*, 1989, **90**, 2154.
- 59 C. Gonzalez and H. B. Schlegel, *J. Phys. Chem.*, 1990, **94**, 5523.
- 60 M. Bonchio, O. Bortolini, M. Carraro, V. Conte and S. Primon, *J. Inorg. Biochem.*, 2000, **80**, 191.
- 61 V. Conte, F. Di Furia and S. Moro, *J. Mol. Catal. A: Chem.*, 1997, **117**, 139.
- 62 V. Conte, F. Di Furia and S. Moro, *J. Mol. Catal. A: Chem.*, 1994, **94**, 323.
- 63 H. Schmidt, I. Andersson, D. Rehder and L. Pettersson, *Chem. – Eur. J.*, 2001, **7**, 251.
- 64 A. E. Gekhman, G. E. Amelichkina, N. I. Moiseeva, M. N. Vargaftik and I. I. Moiseev, *J. Mol. Catal. A: Chem.*, 2000, **162**, 111.
- 65 Y. N. Kozlov, V. B. Romakh, A. Kitaygorodskiy, P. Buglyó, G. Süss-Fink and G. B. Shul'pin, *J. Phys. Chem. A*, 2007, **111**, 7736.
- 66 B. J. Hamstra, G. J. Colpas and V. L. Pecoraro, *Inorg. Chem.*, 1998, **37**, 949.
- 67 G. J. Colpas, B. J. Hamstra, J. W. Kampf and V. L. Pecoraro, *J. Am. Chem. Soc.*, 1996, **118**, 3469.
- 68 A. Butler, *Coord. Chem. Rev.*, 1999, **187**, 17.
- 69 Z. Chen, *Coord. Chem. Rev.*, 2022, **457**, 214404.

